metals

MDPI

Article

Effect of Sb Addition on the Solidification of Deeply Undercooled Ag-28.1 wt. % Cu Eutectic Alloy

Su Zhao *, **Yunxia Chen** and **Donglai Wei**

School of Mechanical Engineering, Shanghai Dianji University, Shanghai 200240, China; chenyx@sdju.edu.cn (Y.C.); wdonglai@163.com (D.W.)

* Correspondence: wellzs@163.com; Tel.: +86-21-3822-6089; Fax: +86-21-3822-3186

Academic Editor: Hugo F. Lopez

Received: 31 December 2015; Accepted: 6 February 2016; Published: 17 February 2016

Abstract: Ag-28.1 wt. % Cu eutectic alloy solidifies in the form of eutectic dendrite at undercooling above 76 K. The remelting and ripening of the original lamellar eutectics result in the formation of the anomalous eutectics in the final microstructure. The addition of the third element Sb (0.5 and 1 wt. %) does not change the growth mode, but enlarges the volume fraction of anomalous eutectics because of the increasing recalescence rate. The additional constitutional supercooling owing to the Sb enrichment ahead of the eutectic interface promotes the branching of the interface and as a result fine lamellar eutectic arms form around the anomalous eutectics in the Sb-added Ag-28.1 wt. % Cu eutectic alloy.

Keywords: eutectic alloys; undercooling; growth modes; microstructure

1. Introduction

Binary eutectic alloys usually solidify into regular lamellar (rod) eutectics under equilibrium solidification conditions [1–3]. With the increase of undercooling, the solidification rate increases and the solidification structures can be composed of a mixture of lamellar eutectics and anomalous eutectics or full anomalous eutectics [4–8]. Furthermore, the rapidly solidified alloys can have a series of good properties, such as high strength and toughness, high temperature creep resistance, electromagnetism and corrosion resistance, *etc.*, because the properties of the as-solidified materials are determined by the conditions under which the liquid solidifies. Therefore, much attention has been paid to the solidification at high undercooling [9–12]. As a small amount of third element is added to a binary eutectic alloy, both a transverse and longitudinal diffusions of the added element in the liquid ahead of the solid-liquid interface is established, due to which the growth behavior changes. However, there have been few experimental investigations on the solidification of eutectic alloys containing a small amount of third element at high undercooling. In this paper, the effect of trace Sb addition on the crystal growth mode and the microstructure of Ag-28.1 wt. % Cu eutectic alloy at high undercoolings will be systematically investigated.

2. Materials and Methods

Three alloys, Ag-28.1Cu, (Ag-28.1Cu)-0.5Sb and (Ag-28.1Cu)-1Sb (weight percent), were investigated. The mass of each alloy sample is 6 g. The high undercooling of the experimental alloys was achieved by glass fluxing method in a high-frequency induction facility [13]. In each experiment, the raw materials (99.999% purity Ag, 99.999% purity Cu and 99.999% purity Sb) were put in a quartz crucible and covered with 0.6 g glass flux. The glass flux consists of 12.3 wt. % B_2O_3, 17.7 wt. % $Na_2B_4O_7$ and 70 wt. % Na_2SiO_3, and was dehydrated at 1273 K for 6 h in advance.

Then, the crucible was placed in the vacuum chamber of a high-frequency induction facility. The vacuum chamber was evacuated and backfilled with ultrapure argon. The raw materials were melted, superheated and cooled through adjusting the input power of the induction coil. To acquire a desired undercooling, it was necessary to repeat the heating-cooling cycle many times with an overheating degree of about 400 K and a holding time of 2–5 min. The power supply was turned off, when the desired undercooling was achieved. Then the sample solidified and cooled to room temperature. All the experimental samples were nucleated spontaneously without any manual triggering. The thermal history of the alloy was monitored by a two-color infrared pyrometer with an accuracy of 1 K and a response time of 1 ms. The sample solidified is a short column with a diameter of about 10 mm.

The phase transformation with temperature was analyzed by differential scanning calorimetry (DSC, Netzsch, Bavaria, Germany). The calibration of temperature and energy scale was performed with pure In and Zn. An argon purge of 80 mL/min was employed for all measurements. Both the heating and cooling rates were 10 K/min.

The phase constitution of the alloy was examined by X-ray diffraction (XRD, Thermo, Waltham, MA, USA). The surface structure of the sample was directly examined without any etching by a scanning electron microscope (SEM, Hitachi, Tokyo, Japan). Then the sample was cut, mounted in epoxy, polished, and etched with a mixture of 4% alcoholic picric acid. The internal structure of the sample was observed by an optical microscope (OM, Olympus, Tokyo, Japan).

3. Results

3.1. Thermal History Analysis

A temperature-time profile recorded in the experiment is shown schematically in Figure 1. When melt is cooled, a temperature decreases to T_N (nucleation temperature) (Stage 1), and at this time, nuclei form, and $\Delta T = T_E - T_N$ (ΔT, undercooling; T_E, eutectic temperature). The latent heat of crystallization released during rapid solidification is absorbed by undercooled melt, which leads to an increase of the temperature, *i.e.*, the so-called recalescence (Stages 2 and 3). During rapid recalescence (Stage 2), the temperature rising rate is faster, crystals grow rapidly and dendrite skeleton forms. Then the coarsening of fine dendritic structures makes the slow recalescence appear (Stage 3). After recalescence, the remaining melt solidifies under near-equilibrium conditions. The solidification during Stage 4 is controlled by the heat transfer from the sample to the environment. Finally, the sample cools to room temperature (Stage 5). Recalescence time, degree and rate refer to the time interval, temperature rise and the rising rate from the start to end of the rapid recalescence (Stage 2 in Figure 1), respectively [14]. Moreover, with the increase of undercooling, recalescence degree decreases and the recalescence time becomes shorter and shorter during rapid recalescence.

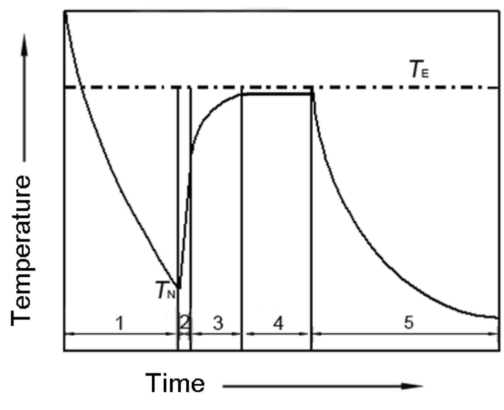

Figure 1. Schematic illustration of a cooling curve during the solidification of undercooled eutectic melt.

3.2. DSC Analysis

At 1054 K the eutectic phase transformation, L → α-Ag + β-Cu, occurs in Ag-28.1Cu alloy [15], indicated by only one endothermic peak during heating and only one exothermic peak during cooling (Figure 2a). With 0.5 and 1 wt. % Sb added to the base alloy, the melting point temperature gradually decreases to 1045 K and 1034 K, respectively, while the heating and cooling curves of the (Ag-28.1Cu)-0.5Sb and (Ag-28.1Cu)-1Sb alloys still exhibit the similar feature with those of the Ag-28.1Cu eutectic alloy (Figure 2b,c).

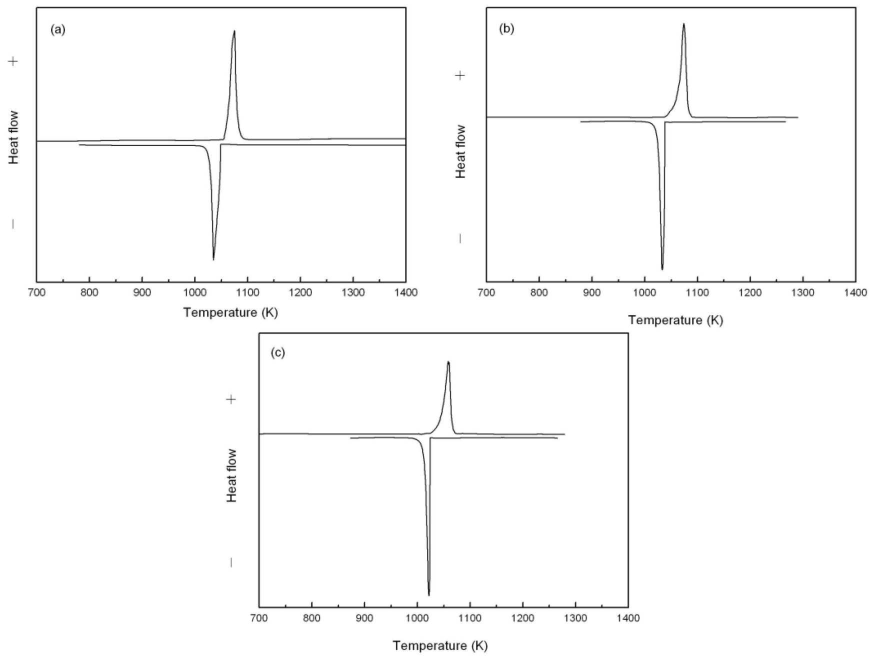

Figure 2. DSC curves of different alloys, (**a**) Ag-28.1Cu, (**b**) (Ag-28.1Cu)-0.5Sb, and (**c**) (Ag-28.1Cu)-1Sb.

3.3. XRD Analysis

Most of Sb can be dissolved in the Ag-rich (α) and Cu-rich (β) phases during solidification to form substitutional solid solutions [16]. Figure 3a,b show that only α-Ag and β-Cu face-centered cubic phases exist in the solidification structures of (Ag-28.1Cu)-0.5Sb and (Ag-28.1Cu)-1Sb alloys, no matter how large the undercooling is. This means that the addition of Sb does not influence the phase constitution of Ag-28.1Cu eutectic alloy.

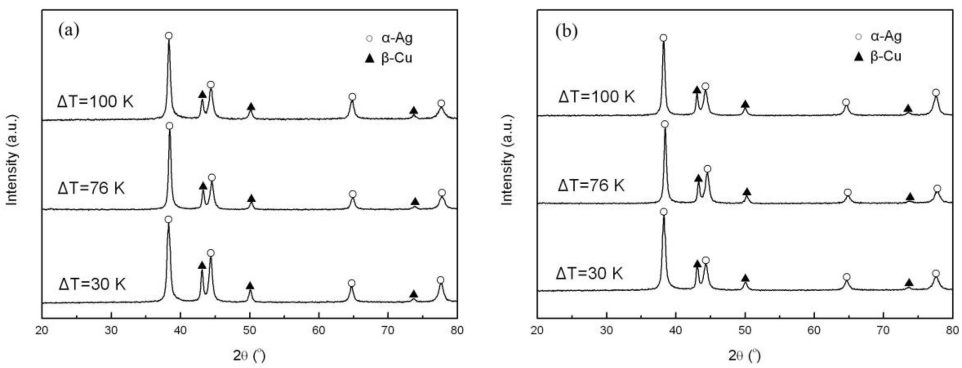

Figure 3. XRD patterns of the alloys Sb-containing solidified at different undercoolings, (**a**) (Ag-28.1Cu)-0.5Sb, and (**b**) (Ag-28.1Cu)-1Sb.

3.4. Microstructures

A large undercooling level up to 100 K can be achieved experimentally in the (Ag-28.1Cu)-*x*Sb (x = 0, 0.5, 1.0) eutectic alloys. Taking 76 K as a critical undercooling, the alloys solidify in a form of cellular eutectics, cellular dendritic eutectics and the undeveloped dendritic eutectics at lower undercooling but dendritic eutectics at larger undercooling. The solidification of the alloys undercooled no more than 76 K has been reported previously [16]. Here, we pay attention to the solidification of the alloys undercooled above 76 K. For Ag-28.1Cu eutectic alloy, developed dendrites on the sample surface are observed under the SEM (Figure 4a). At high magnification, lamellar eutectics are found in the dendrite arms (Figure 4b). Such solidification structures are referred to as eutectic dendrites so as to distinguish them from the dendrites consisting of single phase. For the internal structure, a dendritic morphology is revealed, and the dendrite arms observed are roughly parallel to each other (Figure 4c) and the bright phase has been determined to be rich in Ag, and the dark phase rich in Cu under the OM. But now the dendrite arms are composed of anomalous eutectics and lamellar eutectics around the former (Figure 4d). And the anomalous eutectics refer to the granular particles and fine lamellar fragments [17]. The microstructures of (Ag-28.1Cu)-0.5Sb and (Ag-28.1Cu)-1Sb eutectic alloys are similar to those of Ag-28.1Cu eutectic alloy, as shown in Figures 5 and 6. Their arms are composed of lamellar eutectics on the sample surface but a mixture of anomalous eutectics and lamellar eutectics inside the sample, as occurred in the base alloy, except that the dendrite arms become thinner (Figures 5a and 6a).

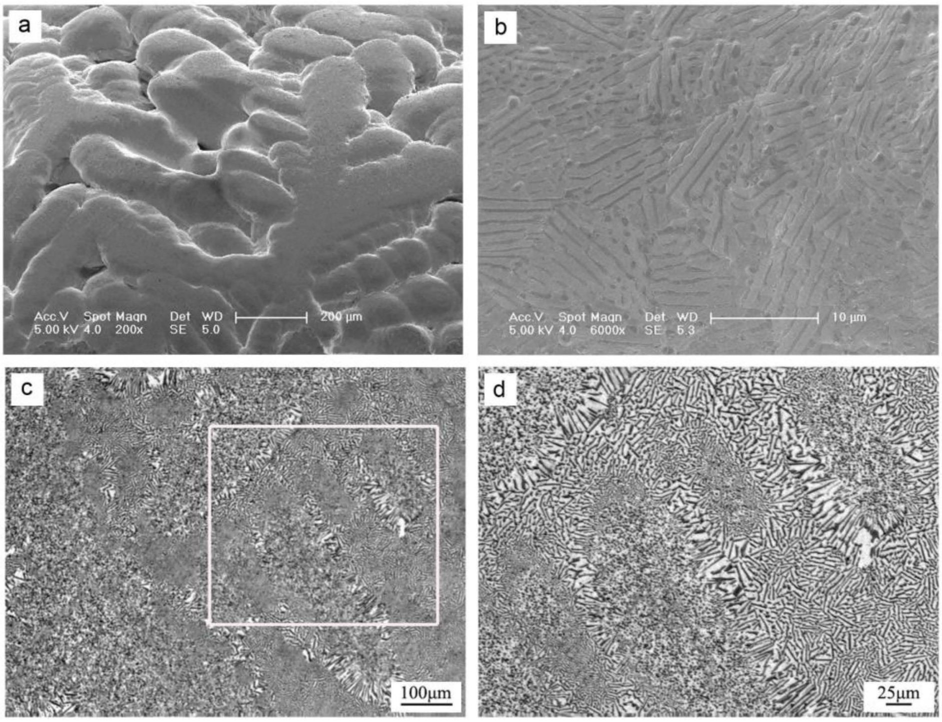

Figure 4. Microstructures of Ag-28.1Cu eutectic alloy undercooled by 85 K, (**a**) the surface structure with dendritic morphology at low magnification, (**b**) lamellar eutectics in the surface dendrite arms at high magnification, (**c**) the internal structure with dendritic morphology at low magnification, and (**d**) anomalous eutectics and the lamellar eutectics around them in the quadrilateral region at high magnification.

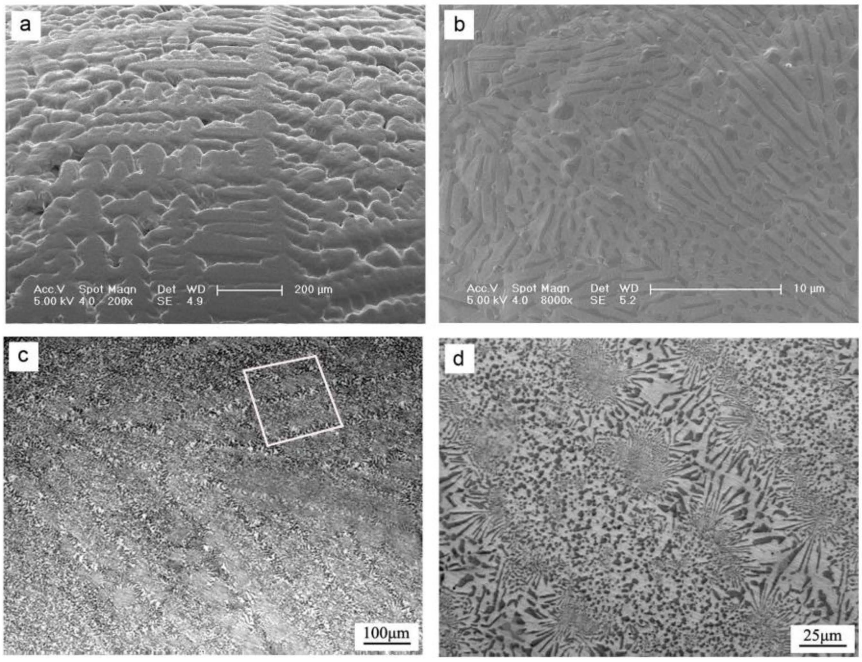

Figure 5. Microstructures of (Ag-28.1Cu)-0.5Sb alloy undercooled by 85 K, (**a**) the surface structure with dendritic morphology at low magnification, (**b**) lamellar eutectics in the surface dendrite arms at high magnification, (**c**) the internal structure with dendritic morphology at low magnification, and (**d**) anomalous eutectics and the lamellar eutectics around them in the quadrilateral region at high magnification.

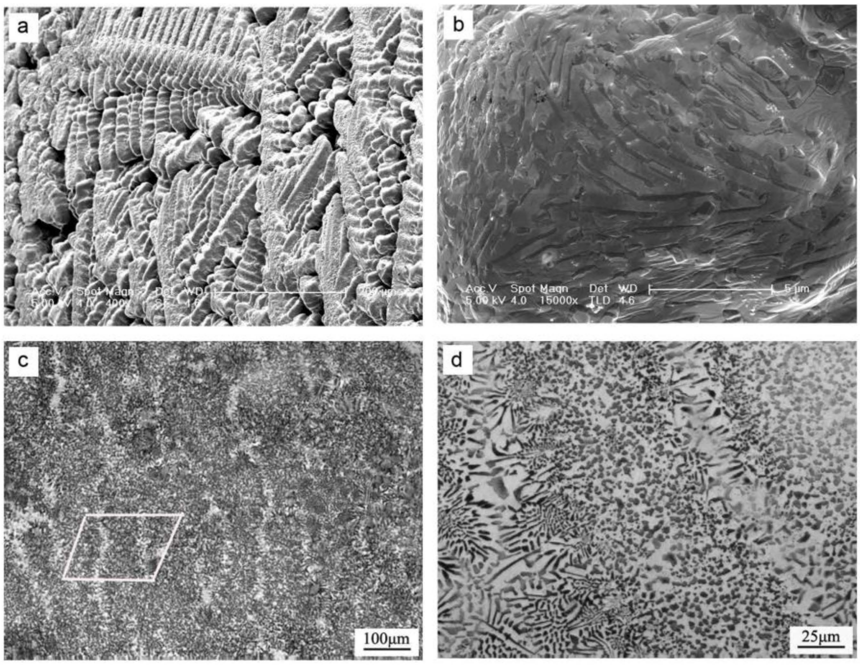

Figure 6. Microstructures of (Ag-28.1Cu)-1Sb alloy undercooled by 85 K, (**a**) the surface structure with dendritic morphology at low magnification, (**b**) lamellar eutectics in the surface dendrite arms at high magnification, (**c**) the internal structure with dendritic morphology at low magnification, and (**d**) anomalous eutectics and the lamellar eutectics around them in the quadrilateral region at high magnification.

The volume fraction of anomalous eutectics at each undercooling was evaluated by measuring the area of the anomalous eutectic zone on the sample cross-section, and the results are shown in Figure 7. It can be seen that the volume fraction increases with the increasing undercooling and the increasing content of Sb.

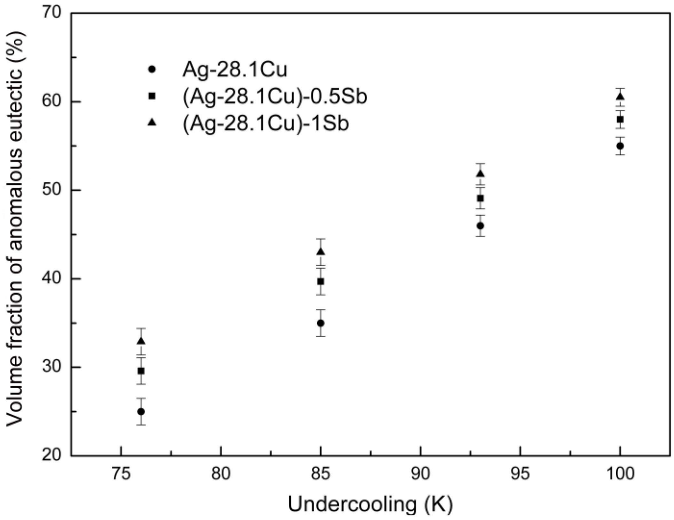

Figure 7. Volume fraction of anomalous eutectic *versus* undercooling for different Sb contents.

3.5. Recalescence Rate

Recalescence time, degree and rate can be used to describe the rapid solidification behavior of undercooled alloy melts. Among them the recalescence rate is directly proportional to the crystal growth rate. The recalescence rates as a function of undercooling at different contents of Sb are shown in Figure 8. It can be seen that the recalescence rate increases with increasing undercooling for the three alloys and at the critical undercooling of 76 K, there is a jump. Furthermore, the higher the Sb content, the larger the recalescence rate.

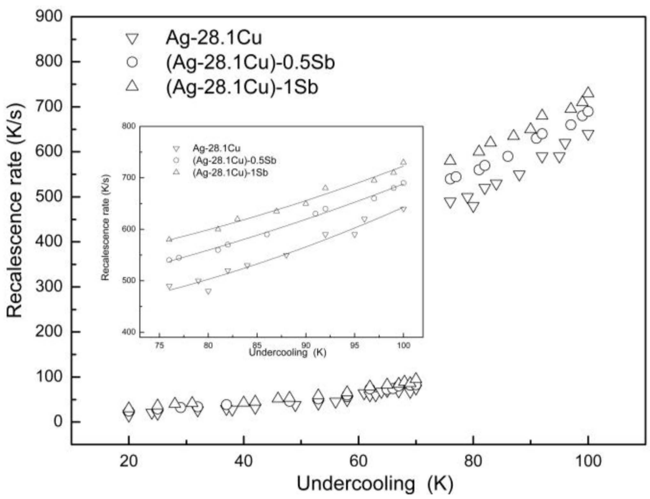

Figure 8. Recalescence rate *versus* undercooling for different Sb contents. The inset is a local amplification.

4. Discussion

4.1. Effect of Sb Addition on the Crystal Growth and the Formation of Anomalous Eutectic

The single-phase dendrite growth in undercooled melts has been well described in the BCT model [18]. According to the BCT model, the physical data of the Ag-Cu eutectic alloy (Table 1) were used to calculate the dendrite growth velocities of α-Ag and β-Cu *versus* undercooling and the results are shown in Figure 9. It can be seen that β-Cu should grow as the primary phase once decoupled growth occurs. For the eutectic dendrite growth in the undercooled Ag-Cu eutectic melt, the growth velocity during rapid solidification can be calculated by the eutectic growth model [19] that has taken the solute trapping into account and been established on the basis of the LZ model [20].

Table 1. Physical parameters of Ag-Cu eutectic alloy [21,22].

Parameter	Value
Latent heat of fusion for α-Ag/β-Cu (J/mol)	11,326/13,027
Specific heat of the liquid (J/mol· K)	32.21
Interdiffusion coefficient of solutes (m^2/s)	$2.42 \times 10^{-7}\exp(-48{,}886/8.314T)$
Volume fraction of α-Ag in the eutectic	0.74
Thermal diffusivity in the liquid (m^2/s)	5.44×10^{-5}
Gibbs-Thomson parameter for α-Ag/β-Cu (m· K)	$1.5 \times 10^{-7}/1.3 \times 10^{-7}$
Eutectic temperature (K)	1053
Liquidus slope for α-Ag/β-Cu (K/at. %)	−4.56/5.07
Kinetic parameter for α-Ag/β-Cu (m/s· K)	0.61/0.71
Equilibrium solute partition coefficient	0.353

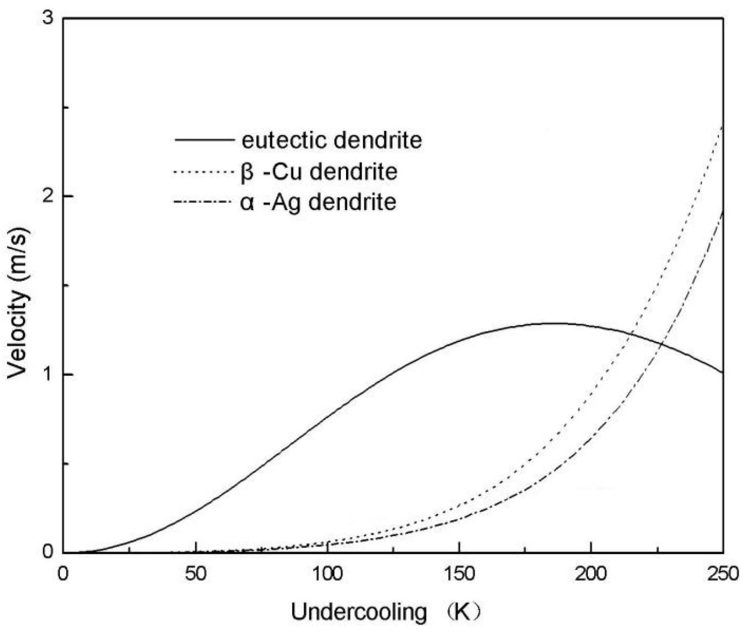

Figure 9. Calculated growth velocities in Ag-28.1 wt. % Cu eutectic melt when eutectic dendrite, β-Cu dendrite or α-Ag dendrite is assumed to form.

The bulk undercooling ΔT at the dendrite tip can be expressed as four terms:

$$\Delta T = m_{\mathrm{v}} a_{\mathrm{v}}^{\mathrm{L}} \frac{1}{\lambda} + m_{\mathrm{v}} \left(V\lambda/D\right) Q_{\mathrm{v}} P\left(f, P_{\mathrm{e}}, k_{\mathrm{v}}\right) + m_{\mathrm{v}} \frac{V}{\mu} + \left(\frac{\Delta H_{\mathrm{f}}}{C_{\mathrm{p}}}\right) Iv\left(P_{\mathrm{t}}\right) \quad (1)$$

Where the parameters are as follows:

$$\frac{1}{m_{\mathrm{v}}}=\frac{1}{m_{\alpha}^{\mathrm{v}}}+\frac{1}{m_{\beta}^{\mathrm{v}}} \tag{1a}$$

$$Q_{\mathrm{v}}=\frac{1-k_{\mathrm{v}}}{f(1-f)} \tag{1b}$$

$$a_{\mathrm{v}}^{\mathrm{L}}=2\left[\frac{\Gamma_{\alpha}\sin\theta_{\alpha}}{fm_{\alpha}^{\mathrm{v}}}+\frac{\Gamma_{\beta}\sin\theta_{\beta}}{(1-f)\,m_{\beta}^{\mathrm{v}}}\right] \tag{1c}$$

$$P\left(f,P_{\mathrm{e}},k_{\mathrm{v}}\right)=\sum_{1}^{\infty}\frac{1}{(n\pi)^{3}}\left[\sin\left(n\pi f\right)\right]^{2}\frac{p_{\mathrm{n}}}{\sqrt{1+p_{\mathrm{n}}^{2}}-1+2k_{\mathrm{v}}} \tag{1d}$$

$$\frac{1}{\mu}=\frac{1}{m_{\alpha}^{\mathrm{v}}\mu_{\alpha}}+\frac{1}{m_{\beta}^{\mathrm{v}}\mu_{\beta}} \tag{1e}$$

where m_i^{v} is the liquidus slope of the α or β phase under non-equilibrium conditions; Γ_i, the Gibbs-Thomson coefficient; λ, the lamellar spacing; f, the volume fraction of the α phase; θ_i, the contact angle; D, the solute diffusion coefficient in the liquid; k_{v}, the solute distribution coefficient under non-equilibrium conditions; $P_{\mathrm{n}} = 2n\pi/P_{\mathrm{e}}$, where solute Peclet number $P_{\mathrm{e}} = V\lambda/2D$; μ, the kinetic parameter; $\Delta H_f = f\Delta H_f^{\alpha} + (1-f)\Delta H_f^{\beta}$, where ΔH_f^{i} (i = α, β) is the heat of fusion; C_{p}, the specific heat of liquid phase; $I_{\mathrm{v}}(P_{\mathrm{t}}) = P_{\mathrm{t}}\exp(P_{\mathrm{t}})E_1(P_{\mathrm{t}})$, the Ivantosv function of thermal Peclet number $P_{\mathrm{t}} = VR/2\alpha$, where α is the thermal diffusion coefficient in the liquid, and R is dendrite tip radius.

Then we calculate the eutectic growth velocities using the physical parameters of Ag-Cu eutectic alloy and the results are also shown in Figure 9. The velocities for β-Cu dendrite and eutectic growths are equal at about 230 K, below which the eutectic dendrite grows faster than β-Cu dendrite. That means the coupled growth of lamellar α-Ag and β-Cu rather than single-phase dendrite growth should take place at the present experimental undercoolings. So the dendritic lamellar eutectics are observed on the sample surface, as shown in Figure 4a,b. Inside the sample, the severe superheating in the primary eutectic dendrites results in the appearance of anomalous eutectics (Figure 4c,d) [23]. When the melt contacts with the crucible wall or glass purifier, the recalescence is depressed greatly. So the eutectic dendrites on the sample surface are retained. On the contrary, inside the sample the temperature can be recalesced close to the eutectic temperature during rapid solidification. Excess solute is trapped in the original lamellar eutectics during rapid solidification because of the large growth velocity and the deviation of the solidification temperature at the solid-liquid interface from the equilibrium eutectic temperature [17,23]. As a result, parts of the original lamellar eutectics are remelted under the action of severe superheating during recalescence. Furthermore, after the recalescence, the broken lamellae decay into anomalous eutectics with granular morphology under the driving force of a reduction of the interfacial energy stored in the fine lamellar eutectics [17].

It is also shown in Figure 9 that when the single-phase dendrite growth occurs, the growth velocity of single-phase dendrite is much greater than that of eutectic dendrite, and for the same growth modes, their growth velocities should rise in the same law with the increase of undercoolings [24,25]. In the present experiment, it is difficult to determine the crystal growth path, so the recalescence rate rather than the growth velocity was measured. The recalescence rate is directly proportional to the growth velocity, so from the results in Figure 8 it is known that the growth velocity rises gradually with the increase of Sb content for a fixed undercooling. Furthermore, the addition of Sb does not change the variation trend of the growth velocity along with undercooling (Figure 8). In addition, perfect eutectic dendrites are formed on the sample surface, but the internal structure are anomalous eutectics and the lamellar eutectics which compose the dendrite arms (Figures 5 and 6), just like the structures of Ag-28.1Cu eutectic alloy (Figure 4). Therefore, it is believed that eutectic dendrite growth also takes place for the eutectic alloys containing Sb. And it is shown in Figure 8 that the growth velocity rises abruptly at the critical undercooling of 76 K. This is in good agreement with the microstructural evolutions: the cellular eutectics (Ag-28.1Cu), cellular dendritic eutectics (Ag-28.1Cu-0.5Sb) and the undeveloped dendritic eutectics (Ag-28.1Cu-1Sb) [16] change into the developed dendritic eutectics at 76 K. The developed eutectic dendrites grow faster, because they have smaller tip radius, which favors the dissipation of the latent heat.

The reduction of tip radius can lead to the increase of recalescence rate [16]. Thus, the composition of the primary eutectics deviates more severely from the equilibrium value, and the more solute is trapped in the primary lamellar eutectics with the rise of recalescence rate [26]. As a result, the volume fraction of anomalous eutectics increases with the increase of both Sb content and undercooling (Figure 7).

4.2. Effect of Sb Addition on the Formation of Lamellar Eutectics

Normally the negative temperature gradient ahead of the solid-liquid interface during solidification in undercooled melt leads to the formation of dendritic morphology [20,27], while planar interfaces are observed in the directional solidification for a pure eutectic alloy [28]. With the proceeding of solidification, the temperature of the undercooled melt increases gradually until it is close to the equilibrium eutectic temperature. The eutectics formed at the stage of slow solidification cannot be remelted and keeps the morphology of regular lamellae because of the fall or disappearance in the supersaturation degree of solute and superheating. So the lamellar eutectics grow outward around the anomalous eutectics for the Ag-28.1Cu eutectic alloy (Figure 4d). For the eutectic alloys containing Sb, however, because the equilibrium partition coefficients of Sb with respect to the both α-Ag and β-Cu phases phases are about 0.46 and 0.31, respectively [15], part of Sb atoms are rejected into the liquid during solidification. As a result, the new solute boundary layer with the enrichment of Sb atoms exists in front of the solid-liquid interface, and a zone of constitutional supercooling is formed. The enrichment of Sb atoms ahead of the interface must be diffused along the direction perpendicular to the interface during solidification, thus destabilizing the planar interface. Therefore, lamellar eutectics with dendritic morphology growing outward around the anomalous eutectics are observed (Figures 5d and 6d).

5. Conclusions

(1) The eutectic dendritic growth takes place in the eutectic alloys containing Sb at the undercoolings ranging from 76 to 100 K. The remelting and ripening of the original lamellar eutectics result in the formation of anomalous eutectics.
(2) For a fixed undercooling, the recalescence rate and the volume fraction of anomalous eutectics increase with the increase of Sb content. For a fixed Sb content, the recalescence rate increases with the increase of undercooling, and there is a jump at 76 K, indicating that the developed eutectic dendrites grow much faster.
(3) The additional constitutional supercooling in the liquid ahead of the eutectic interface caused by Sb addition results in the dendritic growth of lamellar eutectics outward from the anomalous eutectics at the stage of slow solidification of the eutectic alloys containing Sb.

Acknowledgments: This work was supported by National Natural Science Foundation of China, No. 50571068, Research and Innovation Project of Shanghai Municipal Education Commission, No. 14YZ159, Climbing Peak Discipline Project of Shanghai Dianji University, No. 15DFXK02, Shanghai Young College Teacher Training and Financial Assistance Scheme, No. ZZSDJ12006.

Author Contributions: Su Zhao conceived and designed the experiments, analyzed the data and wrote the paper. Yunxia Chen and Donglai Wei performed the experiments.

Conflicts of Interest: The authors declare no conflict of interest.

References

1. Zhu, M.F.; Hong, C.P. Modeling of microstructure evolution in regular eutectic growth. *Phys. Rev. B* **2002**, *66*, 1554281–1554288. [CrossRef]
2. Folch, R.; Plapp, M. Towards a quantitative phase-field model of two-phase solidification. *Phys. Rev. E* **2003**, *68*, 106021–106024. [CrossRef] [PubMed]
3. Xu, J.F.; Liu, F.; Xu, X.L.; Dang, B. Undercooled solidification of Ni-3.3 wt. % B alloy and cooling curve description. *Mater. Sci. Technol.* **2013**, *29*, 36–42. [CrossRef]
4. Han, X.J.; Wei, B. Microstructural characteristics of Ni-Sb eutectic alloys under substantial undercooling and containerless solidification conditions. *Metall. Mater. Trans. A* **2002**, *33*, 1221–1228. [CrossRef]
5. Yang, C.; Gao, J.; Zhang, Y.K.; Kolbe, M.; Herlach, D.M. New evidence for the dual origin of anomalous eutectic structures in undercooled Ni-Sn alloys: *In situ* observations and EBSD characterization. *Acta Mater.* **2011**, *59*, 3915–3926. [CrossRef]
6. Liu, L.; Wei, X.X.; Huang, Q.S.; Li, J.F.; Cheng, X.H.; Zhou, Y.H. Anomalous eutectic formation in the solidification of undercooled Co-Sn alloys. *J. Cryst. Growth* **2012**, *358*, 20–28. [CrossRef]
7. Clopet, C.R.; Cochrane, R.F.; Mullis, A.M. The origin of anomalous eutectic structures in undercooled Ag-Cu alloy. *Acta Mater.* **2013**, *61*, 6894–6902. [CrossRef]
8. Wei, X.X.; Lin, X.; Xu, W.; Huang, Q.S.; Ferry, M.; Li, J.F.; Zhou, Y.H. Remelting-induced anomalous eutectic formation during solidification of deeply undercooled eutectic alloy melts. *Acta Mater.* **2015**, *95*, 44–56. [CrossRef]
9. Li, M.; Nagashio, K.; Ishikawa, T.; Yoda, S.; Kuribayashi, K. Microtexture and macrotexture formation in the containerless solidification of undercooled Ni-18.7 at. % Sn eutectic melts. *Acta Mater.* **2005**, *53*, 731–741. [CrossRef]
10. Xu, J.; Liu, F.; Zhang, D. *In situ* observation of solidification of undercooled hypoeutectic Ni-Ni_3B alloy melt. *J. Mater. Res.* **2013**, *28*, 1891–1902. [CrossRef]
11. Mullis, A.M. The origins of spontaneous grain refinement in deeply undercooled metallic melts. *Metals* **2014**, *4*, 155–167. [CrossRef]
12. Herlach, D.M.; Feuerbacher, B. Non-equilibrium solidification of undercooled metallic melts. *Metals* **2014**, *4*, 196–234. [CrossRef]
13. Liu, N.; Yang, G.C.; Liu, F.; Chen, Y.Z.; Yang, C.L.; Lu, Y.P. Grain refinement and grain coarsening of undercooled Fe-Co alloy. *Mater. Charact.* **2006**, *57*, 115–120. [CrossRef]
14. Wei, B.; Yang, G.C.; Zhou, Y.H. High undercooling and rapid solidification of Ni-32.5% Sn eutectic alloy. *Acta Metall. Mater.* **1991**, *39*, 1249–1258.
15. Subramanian, P.R.; Perepezko, J.H. The Ag-Cu (Silver-Copper) system. *J. Phase Equilibria* **1993**, *14*, 62–75. [CrossRef]
16. Zhao, S.; Li, J.F.; Liu, L.; Zhou, Y.H. Solidification of undercooled Ag-Cu eutectic alloy with the Sb addition. *J. Alloy. Compd.* **2009**, *478*, 252–256. [CrossRef]
17. Goetzinger, R.; Barth, M.; Herlach, D.M. Mechanism of formation of the anomalous eutectic structure in rapidly solidified Ni-Si, Co-Sb and Ni-Al-Ti alloys. *Acta Mater.* **1998**, *46*, 1647–1655. [CrossRef]
18. Boettinger, W.J.; Coriell, S.R.; Trivedi, R. Principles and technologies. In *Rapid Solidification Processing*; Mehrabian, R., Parrish, P.A., Eds.; Claitors Publications: Baton Rouge, LA, USA, 1988; p. 13.
19. Zhao, S.; Li, J.F.; Liu, L.; Zhou, Y.H. Effect of solute trapping on the growth process in undercooled eutectic melts. *Acta Metall. Sin.* **2008**, *44*, 1335–1339.
20. Li, J.F.; Zhou, Y.H. Eutectic growth in bulk undercooled melts. *Acta Mater.* **2005**, *53*, 2351–2359. [CrossRef]
21. Walder, S.; Ryder, P.L. Critical solidification behavior of undercooled Ag-Cu alloys. *J. Appl. Phys.* **1993**, *74*, 6100–6106. [CrossRef]
22. Wang, N.; Cao, C.D.; Wei, B.B. Rapid solidification of Ag-Cu eutectic alloy by drop tube processing. *Acta Metall. Sin.* **1998**, *34*, 824–830.
23. Li, J.F.; Li, X.L.; Liu, L.; Lu, S.Y. Mechanism of anomalous eutectic formation in the solidification of undercooled Ni-Sn eutectic alloy. *J. Mater. Res.* **2008**, *23*, 2139–2148. [CrossRef]
24. Liu, X.R.; Cao, C.D.; Wei, B. Microstructure evolution and solidification kinetics of undercooled Co-Ge eutectic alloys. *Scr. Mater.* **2002**, *46*, 13–18. [CrossRef]

25. Yao, W.J.; Han, X.J.; Wei, B. Microstructural evolution during containerless rapid solidification of Ni-Mo eutectic alloys. *J. Alloy. Compd.* **2003**, *348*, 88–99. [CrossRef]
26. Aziz, M.J. Model for solute redistribution during rapid solidification. *J. Appl. Phys.* **1982**, *53*, 1158–1168. [CrossRef]
27. Goetzinger, R.; Barth, M.; Herlach, D.M. Growth of lamellar eutectic dendrites in undercooled melts. *J. Appl. Phys.* **1998**, *84*, 1643–1649. [CrossRef]
28. Kurz, W.; Fisher, D.J. *Fundamentals of Solidification*, 4th ed.; Trans Tech Publications Ltd.: Dürnten, Switzerland, 1998; p. 108.